PCCP

Contribution of shape resonance and Pt–H EXAFS in the Pt $L_{2,3}$ X-ray absorption edges of supported Pt particles: Application and consequences for catalyst characterization

Dave E. Ramaker,[a] Barbara L. Mojet,*[b]† Marc T. Garriga Oostenbrink,[b] Jeff T. Miller,[c] and Diek C. Koningsberger[b]

[a] *Chemistry Department, George Washington University, Washington, DC 20052, USA*
[b] *Department of Inorganic Chemistry and Catalysis, Debye Institute, Utrecht University, PO Box 80083, 3508 TB Utrecht, The Netherlands*
[c] *Amoco Research Center, E-1F, 150 W. Warrenville Rd., Naperville, IL 60566, USA*

Received 26th January 1999, Accepted 17th March 1999

The electronic and geometric effects induced by hydrogen chemisorption on small platinum particles supported on high surface-area saponite clay and zeolite LTL were studied by near edge X-ray absorption fine structure (XAFS) spectroscopy. A new subtraction procedure was developed to separate the electronic from geometric effects. A significant Pt–H extended X-ray absorption fine structure (EXAFS) scattering (structural effect) was found for energy values between 0 and 20 eV. In addition, the Pt–H antibonding state (electronic effect) was found to produce a shape-resonance and was isolated from the near edge of the L_3 X-ray absorption spectrum. Moreover, for Pt/LTL the shape and energy of the shape-resonance was found to strongly depend on the acidity/alkalinity of the support material, implying a direct influence of the support on the electronic properties of the platinum particles. The results of the study of the resonance state and the Pt–H EXAFS scattering demonstrate the potential of these techniques for characterization of hydrogen chemisorption, metal-promoter, and metal-support effects in catalysis research.

Introduction

The chemical reactivity of small supported metal particles is of considerable fundamental as well as practical interest. Since hydrogen is a reactant in many catalytic processes, understanding the role of hydrogen is critical to obtaining insight into the behaviour of dispersed noble metal catalysts. Unfortunately, the direct observation of H atoms with X-ray diffraction (XRD) or X-ray absorption fine structure (XAFS) spectroscopy is extremely difficult because of the small backscattering cross section for hydrogen. However, it is well known that hydrogen significantly affects the near-edge region of the Pt $L_{2,3}$ X-ray absorption edges. Mansour *et al.*[1] observed that the areas of the Pt $L_{2,3}$ white lines increased with exposure to H_2 in comparison to Pt foil and developed a quantitative technique for determination of the number of unoccupied d-electron states. Lytle *et al.*[2] observed significant changes in white line shape and intensity of the Pt $L_{2,3}$ edges for Pt/SiO_2 heated in H_2 *vs.* He and as a function of temperature. Samant and Boudart[3] noted similar changes in H/Pt *vs.* He/Pt clusters dispersed in Y zeolite. Vaarkamp *et al.*[4,5] showed an effect of interfacial hydrogen between the platinum cluster and the support on the Pt $L_{2,3}$ white line in an attempt to explain the difference in reactivity of γ-Al_2O_3 supported Pt particles as a function of reduction temperature. By comparing experimental data with multiple scattering calculations, Soldatov *et al.*[6] found that H introduced a multiple scattering state in the Pd L_3 white lines of $PdH_{0.6}$. Asakura *et al.*[7] and Reifsnyder *et al.*[8] suggested a new Pt–H resonance state visible in XAFS data after hydrogen adsorption on supported Pt particles. Finally, Boyanov and Morison[9] observed two features in the H/Pt minus Pt foil $L_{2,3}$ difference spectra of Pt clusters supported on zeolite Y and interpreted them as spin–orbit doublets.

Recent *ab initio* electronic structure calculations[10] on noble metal hydrides have elucidated the bonding and antibonding states expected for Pt–H bonding. This does not greatly simplify the interpretation of the Pt near-edge XAFS $L_{2,3}$ data since many other variables besides hydrogen affect the near edge X-ray absorption spectrum. Hydrocarbon reactants[11] and hybridisation[12,13] (affected by metal cluster size) influence the white line. Very recently,[14] it has been shown in our laboratory that the acid–base properties of the support also influence the near edge spectra of the L_3 and L_2 X-ray absorption edges.

The work described in this paper reveals that the observations noted above originate from electronic as well as geometric effects contributing to the $L_{2,3}$ near edge X-ray absorption spectra of platinum. The ability to distinguish between these effects, both induced by hydrogen chemisorption, is critical to understanding the geometric and electronic properties of supported noble metal catalysts. In this work the electronic effects will be separated from the geometric effects by using a novel alignment and difference-spectrum technique based upon subtracting white lines measured on Pt with and without chemisorbed hydrogen. As a result it can be concluded that significant Pt–H extended X-ray absorption fine structure (EXAFS) (dominated by normal H single scattering and exhibiting geometric structure information) is present in the near edge $L_{2,3}$ spectra after chemisorption of hydrogen on

† Present address: Department of Inorganic Chemistry and Catalysis, Eindhoven University of Technology, P.O. Box 513, 5600 MB Eindhoven, The Netherlands

the platinum particles. In addition, a Pt–H shape resonance (dominated by multiple scattering and exhibiting the bonding and electronic structure) is visible in the near edge region of the L_3 X-ray absorption edge of platinum. More importantly, by application of this new procedure, it will be shown for Pt/LTL catalysts that the shape and energy position of this Pt–H shape-resonance is related to the acidity/alkalinity of the support.

The experimental results presented in this paper are the first data to show directly that the support affects the electronic properties of the platinum metal particles. It has been shown previously by our group[15,16] that the catalytic activity of the Pt/LTL, Pd/LTL and Pt/SiO_2 catalysts in the hydrogenolysis of neopentane is also strongly dependent on the support acidity/alkalinity. The results of this study, therefore, imply that the changes in catalytic activity with support acidity/alkalinity are the result of changes in the electronic structure of the platinum particles brought about by the support.

Experimental

Catalyst preparation

The saponite support with the composition $H_{1.2}[Mg_6][Si_{6.8}Al_{1.2}]O_{20}(OH)_4 \cdot nH_2O$ (Si/Al ratio of 5.7) has been synthesised according to Vogels *et al.*[17] Platinum was added by ion exchange at room temperature. First, 85.3 mg of $[Pt(NH_3)_4](NO_3)_2$ was slowly added to the saponite (4.3 g) dispersed in 150 ml water. After 24 hrs the saponite was filtrated, washed and dried at 120 °C. This sample will hereafter be denoted as Pt/Sap6 with 6 the approximate Si/Al ratio.

The acidity of the LTL zeolite supports was varied by either impregnating a commercial K–LTL zeolite with KNO_3 or exchanging it with NH_4NO_3 to give K/Al ratios ranging from 0.63 to 1.25. Each LTL zeolite was calcined at 225 °C and analysed for potassium and aluminium. Platinum was added by incipient wetness impregnation with $[Pt(NH_3)_4](NO_3)_2$ (1.0 wt.% Pt) followed by drying at 120 °C. The catalysts were reduced at 300 °C and passivated at room temperature. The catalysts are designated Pt/LTL(x) with x representing the K/Al molar ratio.

XAFS data collection

The X-ray absorption spectra of the Pt L_3 and L_2 edge of the Pt/LTL catalysts were taken at the SRS (Daresbury) Wiggler Station 9.2, using a Si(220) double crystal monochromator. The measurements were performed in transmission mode using ion chambers filled with Ar to have an X-ray absorbance of 20% in the first and of 80% in the second ion chamber. The monochromator was detuned to 50% maximum intensity at 12250 eV to avoid higher harmonics present in the X-ray beam. The absorption spectra of Pt/Sap6 were taken at the ESRF (Grenoble) BM29 station using a Si(111) double crystal monochromator and with ion chambers with the same type of gas fillings as mentioned above. Samples were pressed into a self-supporting wafer (calculated to have an absorbance of 2.5) and placed in a controlled atmosphere cell.[18] The Pt/Sap6 was dried in flowing He at 250 °C (flow: 100 cm^3 min^{-1}, ramp: 5 °C min^{-1}, hold: 1 h) prior to reduction in flowing hydrogen at 400 °C (flow: 100 cm^3 min^{-1}, ramp: 5 °C min^{-1}, hold: 1 h) and measured under a hydrogen atmosphere at liquid nitrogen temperature (sample denoted by H–Pt/Sap6). Subsequently, the sample was evacuated at 200 °C (1 h) to ensure desorption of all chemisorbed hydrogen. Spectra were taken at liquid nitrogen (LN) temperature under continuous evacuation (sample denoted by Pt/Sap6).

The Pt/LTL catalysts were reduced in flowing hydrogen at 300 °C (flow: 100 cm^3 min^{-1}, ramp: 5 °C min^{-1}, hold: 1 h) and measured under a hydrogen atmosphere at LN temperature (sample denoted by H-Pt/LTL). Following reduction, the samples were treated in a helium flow at 300 °C (ramp: 5 °C min^{-1}, hold: 1 h) to remove chemisorbed hydrogen (sample denoted by Pt/LTL).

EXAFS data analysis

To extract the EXAFS data from the measured absorption spectra, the pre-edge background was approximated by a modified Victoreen curve,[19] normalisation was completed by dividing by the height of the absorption edge, and the background was subtracted using cubic spline routines.[20] The EXAFS were fitted in R–space using the commercially available data analysis package XDAP.[21] The fits were optimised by applying the difference file technique[22] and using phase and amplitude corrected Fourier transforms.[23] The EXAFS data were fit using phase and backscattering amplitudes directly obtained from the experimental EXAFS data for Pt-foil and $Na_2Pt(OH)_6$ *via* Fourier filtering.[4,22]

Theoretical description of the near edge L_2 and L_3 X-ray absorption spectra

The new analysis method of the L_2 and L_3 white line areas is based upon several theoretical concepts, which are schematically viewed in Fig. 1. As illustrated in Fig. 1A the spin–orbit interaction in both the core and valence levels introduce large differences between the L_3 ($2p_{3/2} \rightarrow 5d_{5/2}$, $5d_{3/2}$) and L_2 ($2p_{1/2} \rightarrow 5d_{3/2}$) white lines, both in shape and intensity (the $2p_{3/2}$–$2p_{1/2}$ splitting is around 1709 eV, and the $5d_{5/2}$–$5d_{3/2}$ splitting around is 1.5–2.5 eV).[24] The L_3 edge reflects the empty valence band levels (ΔVB) of both the $d_{5/2}$ and $d_{3/2}$ bands, weighted as $d_{5/2}/d_{3/2} = 6$, however, the L_2 edge reflects only the $d_{3/2}$ level. For small platinum clusters the $5d_{3/2}$ is believed to be completely filled due to band narrowing relative to platinum bulk, therefore, it is assumed that there is no Pt d

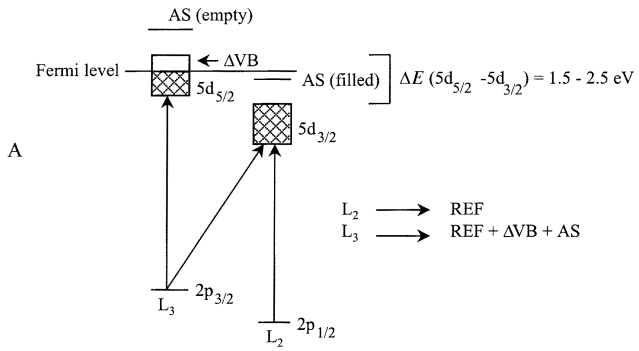

Fig. 1 (A) Illustration of spin–orbit coupling effects in the X-ray absorption $L_{2/3}$ edge spectra and 5d-valence band (B) Illustration of MO picture showing formation of bonding and antibonding orbitals derived from a surface Pt orbital and the H 1s orbital. (C) Matrix summarising major contributions in each absorption edge.

valence band (ΔVB) contribution to the L_2 white line (see further discussion of this below).

Hydrogen chemisorption induces a bonding and an antibonding orbital as reported by Hammer and Nørskov.[10] The partially occupied platinum surface orbitals pointing outward bond to the hydrogen 1s producing the bonding and antibonding Pt–H orbitals. As illustrated in Fig. 1B, the Pt–H bonding orbital is localised more on the H atom, and the antibonding state (AS) is localised more on the surface Pt atoms. Of course, the bonding orbital is occupied so it is not visible in XAS; however, the empty antibonding orbital should be evident in XAS. Thus, the primary effect of the H bonding is to push part of the Pt density of states (DOS) from below the Fermi level to just above the metal Pt valence band into the AS. Since the AS is primarily localised on the surface Pt atoms, and Hammer and Nørskov[10] calculate its position to be approximately 1 eV above the Fermi level, the $5d_{3/2}$ component of the AS is assumed to shift below the Fermi level.

Fig. 1C summarises the important contributions that will be visible, based on these assumptions, in the four X-ray absorption edges: L_3 and L_2 edges with and without hydrogen. The L_2 edge spectrum for Pt clusters without chemisorbed hydrogen can be used as the reference (REF), since this spectrum arises from the "free" atom absorption and the EXAFS contributions. The L_2 spectrum does not contain any valence band contributions as assumed above. The L_2 spectrum for the samples with hydrogen is different from the REF spectrum, because of changes in geometry of the cluster induced by chemisorption of hydrogen (ΔXAFS arising from any additional Pt–H scattering and changes in Pt–Pt and Pt–O scattering). The L_3 spectrum of the Pt cluster without hydrogen contains in addition to REF the electronic (empty part of the valence band: ΔVB) contribution. Finally the L_3 spectrum for the H/Pt sample contains both the geometric (ΔXAFS) and electronic (ΔVB and the chemisorbed hydrogen AS) changes from the reference.

Subtracting the different edges from each other isolates the different contributions: ΔVB, ΔXAFS and AS (this will be further illustrated in the discussion below). The edges, however, have to be properly aligned in order to remove any initial state core level shifts and final state screening effects due to the chemisorption of hydrogen. Moreover, the small differences in normal (Pt–Pt and Pt–H) EXAFS contributions are negligible at the onset of the L_2 X-ray absorption edge. Therefore, the L_2 edges of the samples with and without chemisorbed hydrogen have the same shape at the onset, which allows these L_2 edges to be aligned. Generally, after alignment these edges overlay each other over about 60% of the height of the step–curve with an estimated uncertainty in the alignment of less than 0.1 eV. In practice, the Fermi level of the aligned L_2 edges was arbitrarily placed where the step height of the absorption edges was 0.6. It should be understood that the alignment affects the shapes of the difference spectra, the latter placement of the Fermi level only sets the absolute energy scale relative to the Fermi level.

Since both L_3 edges contain different electronic contributions (ΔVB or ΔVB + AS) they have different onsets. However, the L_3 and L_2 spectra of the same sample have the same EXAFS oscillations, which can be used for alignment of the L_3 edge relative to the L_2 edge. In summary, both L_2 edges were aligned at 0.6 step height, whereas both the L_3 (H/Pt) and the L_3 (Pt) edges were aligned with the help of the EXAFS oscillations relative to the L_2 edges. Thus all edges are aligned relative to the L_2 edge of the sample without chemisorbed hydrogen.

The subtraction technique allows isolation of the AS. This is a localised state embedded in the continuum of the Pt metal cluster. Whenever a localised or bound state (here the AS) is degenerate with a continuum state (here the Pt–H EXAFS wave), the well-known Fano-like spectra profile can be expected due to the auto-ionising probability of this state.[25] The shape resonance, and its effect on the scattering cross-section σ, can be described by the Fano expression:

$$\sigma(E) = 1/kA' \sin^2(\delta + \delta_r)$$
$$= 1/kA' \sin^2\delta \, [\varepsilon - q']^2/[1 + \varepsilon^2], \quad (1)$$

where ε is the normalised energy scale $[\varepsilon = (E - E_{res})/\Gamma]$ relative to the resonance energy, E_{res}, with resonance width Γ, δ_r is the resonant phase shift equal to $\tan^{-1}(-1/\varepsilon)$, q' is the well-known "shape" parameter which accounts for the interference between the resonant and non-resonant waves $[q' = \cot\delta]$, δ is the total phase of the non-resonant cross-section, A' is a normalisation constant, and k is the momentum of the photoelectron. The resonant phase (δ_r) increases rather sharply by an amount π through the resonance width, while the non-resonant phase (δ) and the other parameters are assumed to remain relatively constant over this small width (*i.e.* a few eV).

The total cross-section can be related to the $\chi(E)$ measured in EXAFS *via* the normal relation $\sigma(E) = \mu_o(E)[1 + \chi(E)]$. Rearranging eqn. (1), we obtain

$$\sigma(E) = 2A'/k\{1 + 2\sin(2\delta)[1 - q\varepsilon]/[1 + \varepsilon^2]\} \quad (2)$$

allowing us to make the identification

$$\chi(E) = 1/kA \sin\varphi \, [(1 - q\varepsilon)/(1 + \varepsilon^2)], \quad (3)$$

where we have included all of the constants, the slowly varying $\mu(E)$, and the usual Debye–Waller and inelastic scattering factors found in the usual EXAFS expression into the constant A, and defined the parameter $q = \cot\varphi$ (related to $q' = \cot\delta$ above). Furthermore, φ related to 2δ above, is now the usual phase found in EXAFS containing the $2kr$ term and the phase from the absorber and back-scatterer (*i.e.*, $\varphi = 2kr + 2\delta_a + \delta_b$). A least squares fit of eqn. 3 to the experimentally observed AS lineshape allows a characterisation of the resonance in terms of the parameters φ, E_{res} and Γ.

Results

EXAFS data analysis

The results of the EXAFS data analysis of Pt/Sap6 are given in Table 1. Similar EXAFS analyses of supported Pt clusters in LTL and on other supports have been given previously, so that the quality of the typical fits to χ and the data for similar samples can be seen in this earlier work.[4,12,26] After reduction the average Pt–Pt coordination number is 7.3. After evacuation the Pt–Pt coordination number stays the same within the limit of accuracy. The decrease in Pt–Pt coordination distance by 0.06 Å after evacuation[4] indicates that chemisorbed hydrogen indeed desorbs from the surface. The Pt–O distance of 2.2 Å shows that the interfacial Pt atoms are in direct contact with the saponite support oxygen atoms.[4]

From Table 2 it can be seen that the metal particles in the Pt/LTL series are very small, with Pt–Pt coordination numbers less than 4.5. The long Pt–O distance of approximately 2.68 Å is in accordance with previous studies on Pt/LTL,[26] and is attributed to the presence of interfacial hydrogen. After treatment in helium, only a small contraction occurs in the Pt–Pt and Pt–O distance for all Pt/LTL samples. An additional short Pt–O scattering contribution at 2.26 Å could only be detected for Pt/LTL(0.63).

Analysis of the NEXAFS data for Pt/Sap6

Fig. 2a displays the Pt L_2 and L_3 X-ray absorption edges for H–Pt/Sap6 and Pt/Sap6 as a function of the absolute photon energy (Pt foil data were used as an absolute energy reference). It can be seen that the presence of chemisorbed hydrogen induces large changes in shape and intensity of the white lines

Table 1 Fit parameters (Δk: 3.3–12.5 Å^{-1}, ΔR: 1.80–3.10 Å) and variances for H–Pt/Sap6 and Pt/Sap6

Catalyst	Scatterer	N (±5%)	R Å (±1%)	$\Delta\sigma^2/10^{-3}$ Å^2 (±5%)	ΔE_0 eV (±10%)	k^1-variance (%)[a] Imaginary part	k^1-variance (%)[a] Absolute part
H–Pt/Sap6	Pt	7.3	2.77	0.004	0.3	0.6	0.3
	O	0.4	2.20	0.012	−2.8		
Pt/Sap6	Pt	7.5	2.71	0.007	1.8	0.5	0.2
	O	0.7	2.22	0.015	−2.3		

[a] k^n-variance $= 100 \dfrac{\int [k^n(FT_{\text{model}}(R) - FT_{\text{exp}}(R))]^2}{\int [k^n FT_{\text{exp}}(R)]^2}$

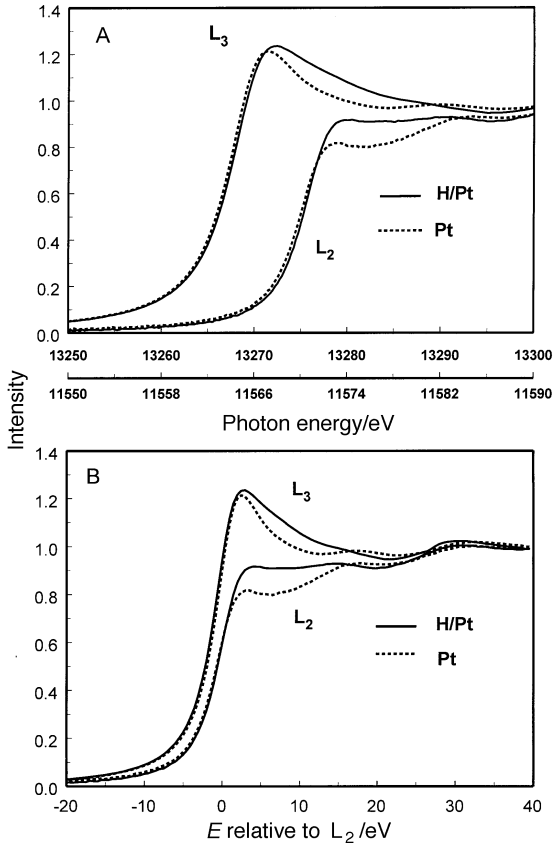

Fig. 2 L_3 and L_2 near edge spectra for H–Pt/Sap6 (reduced at 400 °C, hydrogen chemisorbed solid line) and Pt/sap6 (evacuated at 200 °C, dotted line). (A) As measured (upper scale L_2 ; lower scale L_3) (B) alignment relative to L_2 edge.

of both edges as previously observed.[2–5,7] The L_2 and L_3 edges of Pt/Sap6 appear shifted to lower energies by about 0.2 eV relative to the edges of H–Pt/Sap6.

The results after the alignment procedure as discussed above in the theoretical analysis section are shown in Fig. 2B. The L_2 edges were aligned at 0.6 of the step height and the L_3 edges were shifted so that the L_3 and corresponding L_2 EXAFS oscillations were aligned in the range 50–350 eV after the edge. The L_3 X-ray absorption edge of Pt/Sap6 is now located by about 0.2 eV to the high-energy side of the corresponding edge of H-Pt/Sap6. This is the opposite of that observed in the raw data but occurs as the result of the novel alignment procedure. The physical relevance of this shift is further explained in the Discussion section below.

The separation of the electronic and geometric contributions to the near edge spectra of the Sap6 supported platinum catalysts can now be realised by subtracting the different edges from each other. The difference spectra obtained after subtraction for H–Pt/Sap6 are shown in Fig. 3. The $L_3 - L_2$ edges isolate the electronic contributions: L_3(H–Pt) $- L_2$(H–Pt) $= \Delta L_{3\text{-}2}$(H–Pt) $= \Delta VB + AS$ or L_3(Pt) $- L_2$(Pt) $= \Delta VB$ (Fig. 3a). The difference seen in these two difference spectra clearly reveals the presence of the AS contribution shown in Fig. 3c.

The geometric contribution (ΔXAFS) as a result of hydrogen chemisorption is shown in Fig. 3b: $\Delta L_2 = L_2$(H–Pt) $- L_2$(Pt) $= \Delta$XAFS (thick dashed line). Comparison of the resulting difference curve with a theoretical Pt–H EXAFS function (calculated with the FEFF7 XAFS code[27] assuming a Pt–H distance of 1.8 Å; thin dashed line, Figure 3b) indicates that the ΔXAFS is dominated by Pt–H scattering. The small feature between 20 to 35 eV in the ΔXAFS difference curve is due to the change in the Pt–Pt EXAFS scattering induced by a decrease in the Pt–Pt distance caused by the removal of

Table 2 Fit parameters (Δk: 3.2–14.0 Å^{-1}, ΔR: 1.80–3.10 Å) and variances for H–Pt/LTL and Pt/LTL

Catalyst	Scatterer	N (±5%)	R/Å (±1%)	$\Delta\sigma^2/10^{-3}$ Å^2 (±5%)	ΔE_0/eV (±10%)	k^1-variance (%)[a] Imaginary part	k^1-variance (%)[a] Absolute part
H–Pt/LTL(0.63)	Pt	3.7	2.74	4.6	−2.2	0.7	0.4
	O	2.1	2.69	4.8	7.3		
Pt/LTL(0.63)	Pt	4.2	2.72	4.4	3.1	0.6	0.3
	O	1.0	2.56	2.4	10.6		
	O	0.3	2.26	−6.0	−2.1		
H–Pt/LTL(0.96)	Pt	4.2	2.74	3.5	−1.5	0.6	0.4
	O	1.6	2.69	0.9	4.5		
Pt/LTL(0.96)	Pt	4.3	2.71	4.2	3.4	0.4	0.3
	O	1.1	2.58	−1.4	11.8		
H–Pt/LTL(1.25)	Pt	2.3	2.72	3.3	9.3	0.3	0.1
	O	3.0	2.64	10.5	5.6		
Pt/LTL(1.25)	Pt	2.0	2.70	2.0	6.3	0.3	0.2
	O	1.3	2.61	−1.1	5.6		

[a] k^n-variance $= 100 \dfrac{\int [k^n(FT_{\text{model}}(R) - FT_{\text{exp}}(R))]^2}{\int [k^n FT_{\text{exp}}(R)]^2}$

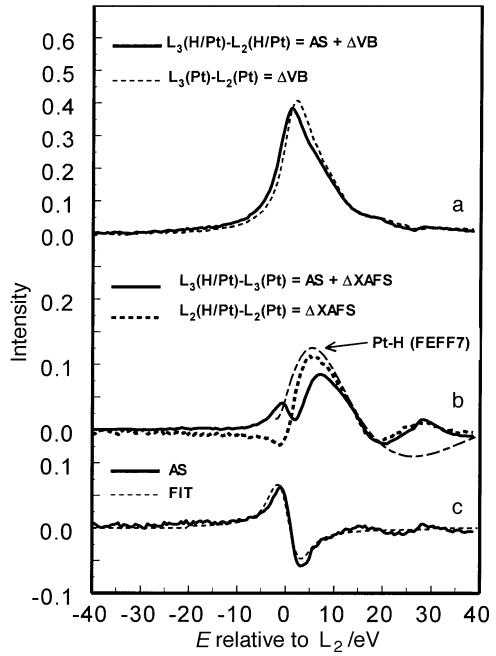

Fig. 3 Results of analysis of near edge spectra of H–Pt/Sap6 and Pt/Sap6: (a) $L_3 - L_2$ difference for H–Pt (solid lines) and Pt samples (dashed lines). (b) $L_3 - L_3$ (solid line) and $L_2 - L_2$ (thick dashed line) difference spectra and Pt–H EXAFS (thin dashed line) as calculated from FEFF7. (c) Subtraction of the difference spectra (solid line) shown in either A or B and Fano profile fit (dashed line) [see eqn. (1)]. Estimated uncertainty in these difference spectra are about ± 0.01 near $E < \pm 3$ eV, and ± 0.005 for $E > \pm 3$ eV. These estimates are based on the observed effects of shifts in the alignment by ± 0.1 eV and the noise level in these difference spectra observed well above $E = 30$ eV.

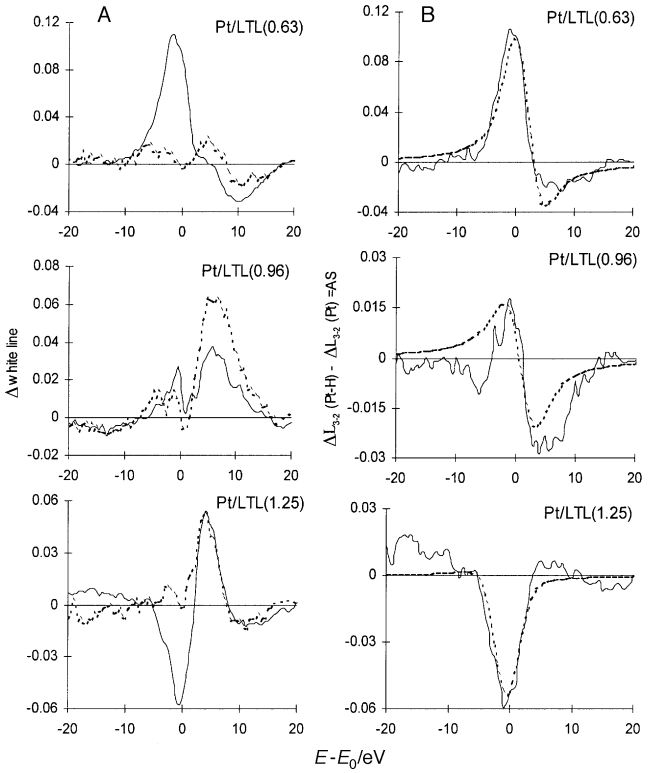

Fig. 4 Results of analysis of near edge spectra of H–Pt/LTL and Pt/LTL: (A) ΔL_3 (*i.e.* AS + ΔXAFS) (solid line) and ΔL_2 (*i.e.* ΔXAFS) (dotted line) for Pt/LTL catalysts. (B) Shape-resonance line shape (*i.e.* AS) for Pt/LTL (solid line) and best fit to resonant lineshape [eqn. (3)] using parameters in Table 3. See Fig. 3 for estimated errors.

chemisorbed hydrogen. The combination of electronic and geometric contributions is also shown in Fig. 3b: $\Delta L_3 = L_3(H–Pt) - L_3(Pt) = \Delta XAFS + AS$ (solid line). The peak around 2 eV in this difference curve again is attributed to the AS state and the peak around 8 eV is due to the presence of the Pt–H EXAFS.

The AS can be isolated by a further subtraction of the difference curves: $\Delta L_3 - \Delta L_2 = \Delta L_{3\text{-}2}$ (H–Pt) $- \Delta L_{3\text{-}2}$ (Pt) = AS (see Fig. 3c, solid line; the difference of the curves in 3a and 3b must be identically equal). The curve representing the solid line in Figure 3c was fit with the Fano profile given in eqn. (3). The optimal parameters are given in Table 3 (parameters α and β are explained below). The theoretical fit was broadened with a 5 eV wide Gaussian to account for experimental and vibrational broadening (the experimental resolution is around 3 eV and the very light H atom will exhibit large vibrational, *i.e.* Debye–Waller type, broadening). The resonance parameters are reasonable considering the expected vibrational broadening and the calculated position of the AS.[10]

Analysis of NEXAFS data for Pt/LTL

The same alignment and subtraction procedure was used to isolate the geometrical and electronic contributions for the Pt/LTL series from the absorption edge spectra. The acidity of the LTL supports changes from acidic [Pt/LTL(0.63)] to neutral [Pt/LTL(0.96)] to alkaline [Pt/LTL(1.25)]. Fig. 4A shows the difference in L_3 and L_2 adsorption edges with and without chemisorbed hydrogen, *i.e.*, $\Delta L_3 = \Delta XAFS + AS$ (solid line) and $\Delta L_2 = \Delta XAFS$ (dashed line). Above 5–10 eV the features in both ΔL_3 and ΔL_2 are similar for all edges, implying that in between 5 and 20 eV single Pt–H scattering primarily dominates the spectrum as also found for Pt on Sap6. Below 5 eV, the differences in the spectra are dramatic and arise from the changing AS in the L_3 edge. Furthermore, these large changes in the AS line shape systematically alter with the acidic or alkaline properties of the support. The double difference spectra of the absorption edges, *i.e.* $\Delta L_3 - \Delta L_2$, isolates the antibonding resonance state (Fig. 4B).

Eqn. (3) was again used in a non-linear least squares fit to the experimental AS line shapes. Also for the Pt/LTL samples a Gaussian broadening of 5 eV was added to account for the experimental resolution and vibrational broadening. Since φ and Γ are strongly interdependent and the width is quite uncertain because of the large broadening, φ and E_{res} are coupled utilising the relation $\varphi = \alpha + \beta E_{res}$ (the physical significance of α and β are discussed below). All 4 resonant line shapes (the 3 LTL and the Sap6 samples) are then fit simultaneously with a total of 14 parameters, *i.e.* E_{res}, Γ, and A for each resonance (each catalyst), plus α and β which are given in Table 3. The dramatic reversal in line shape of the shape resonance with acidity is easily reproduced by the Fano profile (Fig. 4B).

Discussion

Structural information from extended and near-edge XAFS

The results obtained from the EXAFS analysis show that after reduction and in the presence of a hydrogen atmosphere the platinum particles inside the LTL zeolite are very small (4–6 atoms) while the platinum particles supported on Sap6 are larger with approximately 50 atoms per particle.

The contractions of the Pt–Pt distance for Pt/LTL after handling in helium at 300 °C are smaller (about 0.02 Å) than for Pt/Sap6 treated in vacuum at 200 °C (about 0.06 Å). For Pt/Sap6, removal of chemisorbed hydrogen leads to coordinatively unsaturated platinum surface atoms and a smaller Pt–Pt first shell distance.[4] However, the treatment in helium of the Pt/LTL samples leaves He available to physisorb on the

platinum surface, resulting in more coordinatively saturated platinum atoms that may counteract the decrease in Pt–Pt distance upon removal of chemisorbed hydrogen. Therefore, the smaller contractions of the Pt–Pt distance in the Pt/LTL catalysts could occur either because of the incomplete removal of hydrogen or because of the adsorption of He after the hydrogen is desorbed.

The Pt–O distance of 2.2 Å shows that after reduction the interfacial Pt atoms are in direct contact with the saponite support oxygen atoms.[4] This distance stays the same within the limits of accuracy after evacuation at 200 °C. The long Pt–O distance of approximately 2.68 Å on Pt/LTL is in accordance with previous studies[26] and can be attributed to the presence of interfacial hydrogen.[12] For Pt/LTL(0.63) and (0.96) the Pt–O distance decreased by about 0.12 Å due to the He treatment, which is also indicative of a change in the structure of the metal/support interface. However, the He treatment causes a small (0.03 Å) decrease of the Pt–O distance for the Pt/LTL(1.25) sample. It is not clear from these observations to what extent, if any, the interfacial hydrogen is removed for the Pt/LTL samples under the treatment in He at 300 °C. Probably only the chemisorbed hydrogen has been substantially removed in this case.

The change in the shape and intensity of the L_3 and L_2 near edge spectra of all samples provides further experimental evidence for the extent of hydrogen removal. Again, the changes for the Pt/Sap6 sample after evacuation at 200 °C are much larger than for the Pt/LTL samples after treatment in He after 300 °C. This suggests that the less severe conditions for removal of chemisorbed hydrogen with the He treatment indeed result in less hydrogen removed in the Pt/LTL case.

The presence of the interfacial hydrogen in the Pt/LTL case may also have an effect on the cluster, but the interfacial hydrogen is either present before and after the evacuation in the case of the Pt/LTL samples, or absent both before and after for the Pt/Sap6 sample. Thus the interfacial hydrogen should have little effect on the changes we see in Pt–Pt distance or the edge shapes. In any event it should have little affect on the edge analysis since its effects on the spectra will be eliminated during the difference procedure.

Analysis procedure of the near edge spectra

Explanation of alignment procedure. The outcome of the analysis of the L_3 and L_2 near edge spectra depends critically on the alignment procedures. The technique used here is different in two aspects from methods reported in the literature: (i) the edge alignment procedure and (ii) the choice of reference spectrum. Generally, in previous work raw data were left unaligned (or aligned with the help of platinum foil edge spectra) and subtracted from the $L_{2,3}$ edges of platinum foil. However, this introduces both electronic and geometric contributions in the difference spectra due to the broader d-band and higher Pt–Pt coordination number of bulk platinum. Our alignment procedure, based upon the absence (L_2) or presence (L_3) of electronic structure and the use of similar clean Pt cluster data for the reference, avoids these problems. Moreover, the new alignment procedure is particularly suitable to study systems where large shifts (initial or final state effects) are expected (*e.g.* large promoter, metal-support effects and non-metallic clusters). Fig. 5 helps to explain this alignment procedure and illustrates the entire difference method.

The alignment of the EXAFS features of the L_2 and L_3 edge positions the inner potential, E_0 for each spectrum at the same value. The inner potential is the usual parameter used in EXAFS analyses, and is the effective energy reference for the EXAFS features in each spectrum. However, it is important to realise that generally E_0 will be at different energies in the L_2 and L_3 spectra relative to the Fermi level, E_f, as well as relative to the apparent absorption edge. The different E_o arises

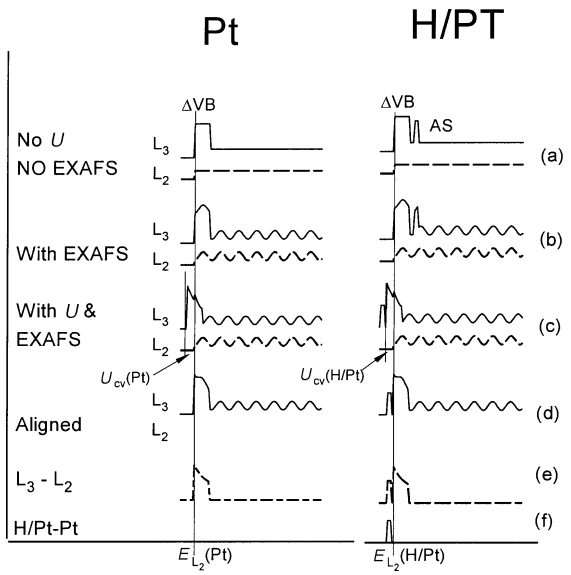

Fig. 5 Illustration of the alignment and difference procedure for both the clean Pt cluster, and with chemisorbed hydrogen. The abscissa indicates the energy relative to the Fermi level, the latter indicated by the vertical lines marked E_{L_2}(Pt) and E_{L_2}(H/Pt) for each case. The difference in these energies constitutes ΔE_{L_2}, the initial state chemical shift as discussed in the text. (a) Schematic density of states showing the continuum (assumed to be the same for the L_3 and L_2 edges) and the "white line" appearing in the L_3 edge. The white line is comprised of the empty valence band (ΔVB) contribution and the Pt–H antibonding state (AS) contribution just above the ΔVB for the H/Pt case. (b) The EXAFS oscillations are now added in assuming the inner potentials (E_0) are the same for the L_3 and L_2 edges. (c) The effects of the core-hole interaction (U_{cv}) as present in the final state of the XAS transition are now included showing that the ΔVB is "pulled down" and distorted in shape, with U_{cv}(Pt) > U_{cv}(H/Pt) as discussed in the text. The illustration shows the AS pulled down below the Fermi level that occurs for the basic Pt supports. U_{cv}(AS) is assumed to be considerably larger than U_{cv}(Pt) or U_{cv}(H/Pt) because the AS is a highly localised orbital mostly on the Pt atom with the core hole. Since E_0 is referenced to the edge, E_o shifts for the L_3 edge in the presence of U_{cv}, causing the oscillations to shift also. (d) Illustration of the alignment procedure which aligns the L_2 and L_3 EXAFS oscillations. (e) The difference $L_3 - L_2$ recaptures the distorted ΔVB and AS contributions. (f) The difference H/Pt − Pt recovers the AS state, although pulled down in energy by the large U_{cv}(AS) present in the XAS final state". We have ignored here the interaction of the AS with the EXAFS continuum that causes the AS to ultimately exhibit a Fano spectral profile. Although not specifically drawn, this schematic also illustrates that the difference L_3(H/Pt) − L_3(Pt) would contain ΔVB + ΔXAFS, and L_2(H/Pt) − L_2(Pt) equals ΔXAFS.

because of the difference in character between the XAS final states at these two edges. The L_3 has a white line while the L_2 does not, making it impossible to identify the same reference or edge point, and the positions of E_o for the L_2 and L_3 final states are actually different. Furthermore, the position of E_0 can vary with the chemistry; as in our case, absence or presence of chemisorbed H.

When an electron is excited from the core level at binding energy E_c (relative to E_f) into some final state, call it E_v, the required photon energy, hν, is $E_c - E_v - U_{cv}$ where U_{cv} is the core-hole electron attraction. The core-hole electron attraction energy enters, because the final state rule dictates that it is the final density of states (*i.e.* the one with the core-hole) that is reflected in the spectral lineshape.[28] We need to consider the magnitude of this attraction energy for all four different cases; namely at the L_2 and L_3 edges for clean Pt and H/Pt. At the L_2 edges, when the electron is excited into the continuum involving the diffuse Rydberg type orbitals, and assuming the valence band is full, U_{cv} will be negligible and we have the edges E_{L_2}(Pt) and E_{L_2}(H/Pt) as shown in Fig. 5. Consequently, the shift in the energy ΔE_{L_2} required for alignment of the L_2 edges can be regarded as an initial state chemical shift,

$\Delta E_{L_2} = E_{L_2}(\mathrm{Pt}) - E_{L_2}(\mathrm{H/Pt})$. This shift is very small since the core levels are hardly influenced by hydrogen chemisorption (of the order of a few tenths of eV), and therefore within experimental error. In Fig. 5, we have assumed for convenience that E_0 and E_f are at the same position at the L_2 edges.

At the L_3 edges, when the electron is excited into the valence band near the edge involving the more localised valence-band orbitals, U_{cv} will be significant, amounting up to 1 eV or even more in very small clusters where the metallic character is limited. Furthermore, this core-hole electron interaction can change significantly with the electron density on the Pt cluster, since the other electrons can screen this interaction. Thus, the L_3 edges will fall at $E_{L_3}(\mathrm{Pt}) = E_{L_3}(\mathrm{Pt}) - U_{cv}(\mathrm{Pt})$ and $E_{L_3}(\mathrm{H/Pt}) = E_{L_3}(\mathrm{H/Pt}) - U_{cv}(\mathrm{H/Pt})$. Alignment of the L_3 spectra is accomplished by aligning the corresponding EXAFS features with the L_2 spectra. The relative shift is $\Delta E_{L_3} = E_{L_3}(\mathrm{Pt}) - E_{L_3}(\mathrm{H/Pt}) - U_{cv}(\mathrm{Pt}) + U_{cv}(\mathrm{H/Pt}) = \Delta E_{L_2} - \Delta U_{cv}$. The shift $-\Delta U_{cv}$ can be regarded as a final-state-screening shift.

Since the change in the core-hole electron attraction can be significant with chemical changes, the relative shift ΔE_{L_3} can be relatively larger (up to one eV) than the ΔE_{L_2}. For Pt/Sap6, the upward shift (*e.g.*, shift to the right in Fig. 5 and 2) of the L_3 edge for the clean Pt edge relative to the H/Pt edge is 0.4 eV. This is enough to reverse the order of the L_3 edges, evident when comparing Fig. 2A with 2B. The relatively smaller upward shift of the H/Pt edge is expected because the hydrogen adsorption allows the Pt–Pt distance to return to bulk values as exhibited in the EXAFS data, and hence the cluster becomes more metallic like. This allows more screening which reduces the core-hole electron interaction [i.e. $U_{cv}(\mathrm{Pt}) > U_{cv}(\mathrm{H/Pt})$]. Furthermore, it is consistent that the ΔE_{L_3} required for Pt/LTL is much smaller than that for Pt/Sap6. For the LTL zeolites, the "clean" Pt surface is believed to have interfacial hydrogen still present as well as He (and perhaps some remaining chemisorbed hydrogen) on its surface, and is, therefore, more metallic-like than for the completely evacuated Pt/Sap6. This allows the Pt–Pt distance to stay relaxed to nearly bulk values before and after the chemisorbed hydrogen removal (this is clearly exhibited in the EXAFS results, which shows much smaller changes in Pt–Pt distance for the LTL). Therefore, the difference in the core-hole electron interactions for the clean Pt and H/Pt cases is also much smaller for the LTL. Finally, the order of the experimental edge energies for a clean Pt cluster, H/Pt cluster, and bulk Pt (clean Pt < H/Pt < bulk) is also consistent with this picture since the screening should be most efficient in bulk Pt.

Assumptions regarding filled $5d_{3/2}$VB. Some additional comments need to be made regarding the assumption of a completely filled $5d_{3/2}$ VB. First, it should be noted that by VB, the more localised d-orbital part is indicated (this should be clear from Fig. 2B), not the delocalised s and p part of the VB, which surely has some part unoccupied. Calculations reported by Matheiss and Dietz[24] for bulk Pt indicate that out of 10 possible d electrons per Pt atom, only 0.34 holes exist per Pt in the 3/2 valence band compared with 1 hole per Pt in the 5/2 band. It is well known that band narrowing occurs in the small Pt clusters such as studied in this work, so this will reduce the $d_{3/2}$ hole number even further, if not to zero. Moreover, the procedure utilised here is not dependent on the absence of empty d-states at the L_2 edge, since then $L_3(\mathrm{Pt}) - L_2(\mathrm{Pt})$ would represent the difference in unoccupied states without any fundamental difference in interpretation.

If the AS were partially unoccupied in the L_2 case, then the $L_3(\mathrm{H/Pt}) - L_2(\mathrm{H/Pt})$ difference would represent $\Delta\mathrm{AS} + \Delta\mathrm{VB}$, and ΔAS might be altered from the Fano profile. However, (i) the striking similarity in the low energy part of the L_2 edge for Pt and H/Pt, and (ii) the remarkable agreement between the Pt–H (FEFF7) theoretical curve and the $L_3(\mathrm{H/Pt}) - L_2(\mathrm{Pt}) = \Delta$XAFS difference (to be discussed below), points very clearly to the lack of a significant AS contribution in the L_2 edge for the very small Pt clusters examined here. Moreover, the procedure here does not become invalid should the band not be completely filled. For example, for Ir clusters currently under study by our group, the $d_{3/2}$ band is not completely filled, and the AS state is not filled at the L_2 edge, but the ΔAS as determined by the subtraction procedure still appears Fano-like.

Pt–H EXAFS and number of empty d-states (ΔVB)

The striking agreement between the Pt–H (FEFF7) theoretical curve and the $L_3(\mathrm{H/Pt}) - L_2(\mathrm{Pt}) = \Delta$XAFS difference as shown in Fig. 3b strongly suggest that the peak around 5–8 eV indeed can be attributed to Pt–H EXAFS. The observation of substantial Pt–H EXAFS scattering below 20 eV is significant since it may allow the Pt–H bonding distances and coordination number to be determined. The backscattering cross-section of hydrogen is only significant at low electron kinetic energies because scattering is primarily resonant, and hydrogen has only the relatively low binding 1s electrons. In the normal EXAFS analysis procedure, where the Fourier transform of χ is typically taken from $k = 3$–14 Å^{-1}, this Pt–H EXAFS scattering is almost completely missed.

The width of the isolated valence band (ΔVB) of about 10 eV is much larger than the calculated width of the unoccupied DOS (<1 eV). The experimentally observed width, however, is due to (i) experimental resolution (3–5 eV) and (ii) hybridisation of the d orbitals with the s, p valence orbitals. This hybridisation should change with particle size; indeed comparisons (not shown here) of ΔVB for bulk Pt foil with that for the small particles in the Pt/LTL case show understandable differences. However, the broadening due to resolution is too large and the clusters are too small to allow conclusions to be drawn about the change in ΔVB for the different particles and supports in this study. More systematic investigations are necessary to fully explore the potential of the Pt–H EXAFS and ΔVB to be used as new tools for structure determination.

Characteristics of the shape resonance

A shape resonance results from a bound state degenerate with continuum states, thereby having a finite lifetime. The AS functions as a temporary bound state for photoelectrons before they are ejected to the continuum. When the photoelectron is excited to the AS in the continuum, the electron can temporarily reside in the resonance bound state above the Fermi level. From the scattering viewpoint this introduces multiple scattering contributions, which add in phase at low energy to a positive peak, while they cancel out at higher energies due to the phase differences resulting from the different scattering lengths. In this way, multiple scattering features can describe an "electronic-like" AS in the X-ray absorption spectrum. The Fourier transformation of this peak will result in a broad background like signal in the radial distribution function; *i.e.*, it will not yield a peak that can be attributed to a single scattering length.

The resonance energy, E_{res}, systematically drops in energy from plus to minus with increasing alkalinity for the Pt/LTL system. The negative resonance energy for the alkaline catalysts with respect to the edge may in part be caused by our initial choice of E_0 at 0.6 times the step-edge of the L_2 Pt spectrum; *i.e.*, E_0 may not necessarily be at the actual Fermi level of the cluster. However, much more important, the negative E_{res} results because the resonance (localised primarily on the Pt atom with the core hole) is pulled down below the Fermi level by the core-hole electron attraction, as illustrated in Fig. 5. Consistent with the final state rule,[28] the values of E_{res} do not reflect the actual energy of the AS in the ground

state but in the presence of a core hole. Although the Sap6 support is believed to be considerably more acidic than LTL(0.96), the E_{res} does not fall between LTL(0.63) and LTL(0.96). However, the Pt particles on Sap6 are much larger than for the LTL systems, and the nature of the Pt–H bond may change with particle size due to the increased metallic nature of the larger particles.

From electron scattering theory, the natural width of the resonance (Γ) is determined by the magnitude of the quantum mechanical matrix element, V, involving the Pt valence band and the Pt–H AS, that is $\Gamma = 2\pi V^2$. In the limit of large V, the resonance would become invisible because of its extremely large width, *e.g.*, it becomes part of the continuum. In the limit of small V, the experimental resolution and vibrational broadening would determine its actual width. Table 3 shows a systematic change in the width of the resonance with E_{res}; as E_{res} decreases, the width initially increases. This obviously occurs because the increasing degeneracy or overlap of the resonance with the Pt VB increases V and enables faster autoionisation of the resonant electron. However, as expected, the resonance width dramatically decreases when the AS drops close to and below the Fermi level [for Pt/Sap6 and Pt/LTL(1.25)], since now the electron cannot escape into the degenerate Pt filled orbitals.

The intensity factor A reflects the magnitude of the backscattering factor, the Debye–Waller factor, the amount of 5d Pt DOS involved in the Pt–H bonding, and the extent of hydrogen removal. The extent of hydrogen removal is also directly reflected in the magnitude of the H EXAFS peak. Therefore, the larger value of A for Sap6 is consistent with the larger H EXAFS amplitude (0.11 compared with $\approx$0.02–0.05 for the LTL). It apparently rises because of a more complete removal of hydrogen from the Sap6 supported platinum particles, presumably because the Sap6 sample was heated *in vacuo* while the LTL zeolite was heated in He. The amplitudes (A) are the same for LTL(0.96) and LTL(1.25) to within the uncertainty of the data and fitting procedure consistent with the similar amplitudes of the H EXAFS peaks. The larger A value for LTL(0.63) does not reflect a larger H removal (its H EXAFS peak is the smallest of the 4 cases); therefore, it may reflect a number of other factors such as a smaller Pt–H distance or changed Debye–Waller factor, *etc.*; conditions which may be changing as the acidity of the support increases.

The background phase parameter, φ, is assumed to be proportional to E_{res} in the expression $\alpha + \beta E_{res}$. Here β includes the entire energy dependence of the total background phase $2kR + 2\delta_a + \delta_s$ (the latter indicate the phase of the absorber and the scatterer). FEFF7 calculations for Pt–H scattering shows that indeed φ varies linearly with energy at lower energies, giving the phase $\varphi = -0.5 + 0.37E$ for a Pt–H distance of 1.8 Å, and as shown in Fig. 3b, the FEFF7 code reproduces the experimental Pt–H EXAFS $\chi(E)$ even at these low energies. The optimal fit of eqn. (3) to the AS line shapes, gives $\beta = 0.38 \pm 0.03$ in excellent agreement with the FEFF7 results. The optimum α parameter at -0.3 ± 0.1 is reasonable compared to -0.5 obtained with FEFF7, since it depends on the inner potential E_0, which is never predicted very accurately by the FEFF7 code.

The φ parameter not only changes the shape of the resonance through the parameter q, but also its intensity through the sin φ factor out front. Therefore, the maximum intensity, $I_{FanoRes}$ is actually

$$I_{Res} \approx A(\sin\varphi + 1/2\cos\varphi) \propto I_{H\text{-}EXAFS} \times [\sin(\alpha + \beta E_{res}) + 1/2\cos(\alpha + \beta E_{res})] \quad (4)$$

where we have assumed that the extent of H removal, as reflected in the intensity of the H EXAFS peak ($I_{H\text{-}EXAFS}$), is the dominant factor determining A. An attractive feature, E_{res} varies systematically with the acidity of the support. However, a non-linear least squares fit of the Fano profile to the experimental data is required to determine E_{res}, since the exact value of E_{res} is not visually obvious from the line shape. This is because the line shape does not cross the axis at $\varepsilon = 0$ (which would give E_{res}), but rather at $\varepsilon = 1/q$. According to eqn. (4), in the region of the observed resonances, $E_{res} = \pm 2$ eV, the ratio $I_{Res}/I_{H\text{-}EXAFS}$, should vary monotonically over a rather large range. Here, I_{Res} is the extreme (maximum or minimum, depending on the line shape, around $E - E_o = 0$) of the resonance feature in the ΔL_3 difference curve, and $I_{H\text{-}EXAFS}$, is the maximum intensity of the Pt–H EXAFS feature in the ΔL_2 difference curve. For example, from Fig. 3b the Pt–H EXAFS peak in the ΔL_2 spectra has intensity 0.11 while the shape resonance peak in the ΔL_3 has intensity 0.063 giving a ratio of 0.57 (this ratio is tabulated for all of the 4 cases in column 6 of Table 3). This ratio varies not only systematically with the acidity of the support, but over a much larger range than E_{res}, and it is much more obvious from a visual inspection of the resonance line shape.

Shape resonances as reported in the literature

The analysis of the L_3 and L_2 near edge spectra of supported platinum catalysts with and without hydrogen can be compared with those previously given in the literature (Table 4). Asakura *et al.*,[7] and Reifsnyder *et al.*[8] previously assigned the entire residue in the difference spectra to a Pt–H shape resonance, assigning both the negative and positive going peaks to the same resonance profile. Boyanov and Morrison,[9] assigned the first peak (<5 eV) to an AS; however, these authors assigned the second peak (3–10 eV) to a second resonance arising from the same AS (a split spin–orbit doublet). This assignment has several problems, already recognised by the authors. While the second peak has a strong temperature dependence (as shown in their work) the first peak does not. If the two peaks form a doublet they should exhibit the same temperature dependence. If the first peak is an antibonding "electronic" state, it should not have the same temperature dependence as the H-EXAFS feature. Further, the splitting found for the two peaks (5 eV) is too large to be caused by the valence band d-level spin–orbit coupling in Pt (1.5–2.5 eV) as discussed by Boyanov and Morrison,[9] Soldatov et al.[6] showed that the intensity of the first peak was sensitive to the projection of angular momentum (m_l=0, 1, 2), which is fully consistent with the behaviour of a highly directional AS. On the contrary, his second peak changed very little with m_l, which is consistent with a single scattering EXAFS phenomenon. Thus,

Table 3 Resonance parameters obtained from non-linear least squares fit of Fano profile expression to the hydrogen induced shape resonance in experimental spectra utilising $\varphi = \alpha + \beta E_{res}$: with optimal $\alpha = -0.3 \pm 0.1$ and $\beta = 0.38 \pm 0.02$

Catalyst	A ($\pm$0.03)	E_{res}[a]/eV ($\pm$0.3)	Width, Γ[b]/eV ($\pm$0.4)	φ (calc.) ($\pm$0.1)	$I_{Res}/I_{H\text{-}EXAFS}$ ($\pm$.05)
H–Pt/Sap6	0.15	0.6	1.9	−0.06	0.57
H–Pt/LTL(0.63)	0.15	2.0	2.1	0.47	5.0
H–Pt/LTL(0.96)	0.04	1.1	3.4	0.10	0.42
H–Pt/LTL(1.25)	0.08	−1.2	1.2	−0.76	−0.15

[a] Relative to the L_2 absorption edge. [b] Resonance width. A 5 eV Gaussian broadening, to account for experimental resolution, was also applied.

Table 4 Comparison of previous interpretations with that from this work

Ref.	First feature (<5 eV)	Second feature (3–10 eV)
This study	Antibonding shape resonance (multiple scattering dominated)	Pt–H XAFS (single scattering dominated)
7 and 8	Single antibonding resonance due to H	Single antibonding resonance due to H
9	Doublet antibonding resonance due to H	Doublet antibonding resonance due to H
6	Pd-density of states change	Pd-H multiple scattering feature

Soldatov *et al.*[6] did observe the proper trends in their calculations, but did not arrive at the correct interpretation.

Shape resonances in near edge X-ray absorption spectra are very well known in molecules, for example, the antibonding π and σ intra-molecular resonances are commonly used to determine the orientation of molecules absorbed on surfaces (see, for example, the book by Stohr[29]). It has been shown recently[30] that similar resonances can be seen on the surface of SiC; the first example of a shape resonance in NEXAFS arising from a localised AS at a clean solid surface. Finally, shape resonances have been identified for antibonding orbitals between a surface atom and an atomic adsorbate; including the metal–H interaction as discussed immediately above. The important aspect of the present work is the technique for separation of the geometric and electronic effects of the metal–H bonding allowing (i) the important identification of Pt–H EXAFS contributions, and (ii) the quantitative fit to a Fano profile of the AS induced by hydrogen chemisorption.

Perhaps the most convincing argument for the identification of the shape resonance is the systematic increase in the magnitude of the resonant lineshape with H coverage while keeping either the same resonant lineshape or a systematically varying lineshape. This is seen: (i) in the data reported here, where the LTL and Sap6 data fit into a systematically changing lineshape based on the acid–base properties of the support in spite of the significantly different amounts of H removed and (ii) perhaps even more convincing in the data of Asakura *et al.*,[7] where indeed the lineshape remains constant, while the intensity increases with H coverage on Pt particles. Further, the fact that all of the other resonance parameters, the energy, width, and background phase, change exactly as expected from theory with support acidity, is very strong evidence for the existence of the resonance.

Metal-support interaction and catalytic properties

The turnover frequency (TOF) for neopentane hydrogenolysis for Pt/LTL, Pd/LTL and Pt/SiO_2 catalysts is strongly dependent on the acidity/alkalinity of the support.[15,16] As discussed above, the characteristics of the shape resonance are also strongly influenced by the acid–base properties of the support. The change in relative positions of the Fermi level and AS for the three LTL catalysts is consistent with observations from XPS and FTIR spectroscopy.[14,15,16] XPS on Pd/LTL showed a decrease of the Pd 3d binding energy with increasing alkalinity (by 1.4 eV from acidic to alkaline Pd/LTL)[14,15] pointing to an increased electron screening with alkalinity or a shift of the Fermi level to lower binding energy. FTIR showed a systematic decrease in the linear to bridge bonded ratio of chemisorbed CO with increasing alkalinity of the support, pointing to a higher electron backdonation from the d-orbitals.[31] The decrease (from positive to negative) in E_{res} with increasing alkalinity is also consistent with an increase in the energy of the Pt Fermi level or decrease in Pt electronic affinity with support alkalinity. Furthermore, since the energy of the H 1s orbital is lower than the Pt Fermi level, the 3.2 eV decrease in E_{res} from acidic to alkaline LTL supports also suggests that the energy of the AS decreases resulting in a weaker Pt–H bond with alkalinity. The data for the larger Pt particles on Sap6, also suggest that the Pt–H bond should decrease in strength with particle size. Consistently then, this work suggests that the Pt–H bond strength decreases with the metallic nature of the particle, either due to the metal support interaction or the particle size. In the future, determination of the position of the resonance state for an adsorbed hydrocarbon, such as neopentane, could give deeper insight in the precise effect of the influence of the metal electronic structure on the catalytic properties as induced by the interaction with the support.

Conclusions

In summary, the geometric (Pt–H EXAFS) and electronic (AS resonance and ΔVB) effects of hydrogen chemisorption on Pt clusters have been isolated utilising a novel edge subtraction procedure. These results demonstrate the potential of the near edge XAFS to study H adsorption, both electronic and geometric affects. In addition, the ΔVB information, although not used extensively in this work, gives new opportunities to investigate hybridisation (cluster size) and other geometric effects, perhaps those not even observable with the normal EXAFS analysis. Perhaps most exciting, our results reveal that the Fano profile parameters vary systematically with the alkalinity of the support, revealing for the first time a direct influence of the support on the electronic properties of the metal particles.

The techniques utilised here certainly are not limited to hydrogen adsorption. It is anticipated that these techniques can be used to study all types of atomic adsorption (*e.g.*, oxygen, nitrogen, *etc.*) and even perhaps molecular adsorption if relatively strong bonding and antibonding orbitals are formed. It is anticipated that the resonance state, as well as the Pt–H EXAFS scattering, can be used as new tools to study the role of hydrogen, metal-promoter and metal-support effects in noble metal catalysts. Furthermore, these techniques are applicable to a wide array of other systems where atoms and molecules adsorb on surfaces, such as in electrochemistry, fuel cells, *etc.*, and even more generally in bulk solids, where specific antibonding resonances can be identified, such as in biological systems.

No measurement can more directly reflect the critical metal–adsorbate interaction, than observation of the bonding and antibonding orbitals constituting that interaction. The ability to detect the metal–adsorbate antibonding orbitals and determine the systematic variation in energy with the alkalinity of the metal support, in a wide range of catalytic systems even under reaction conditions, indicates the many potential applications of the analysis methods presented in this paper.

References

1 A. N. Mansour, J. W. Cook Jr. and D. E. Sayers, *J. Phys. Chem.*, 1992, **96**, 4690.
2 F. W. Lytle, R. B. Greegor, E. C. Marques V. A. Biebesheimer D. R. Sandstrom, J. A. Horsley, G. H. Via and J. H. Sinfelt, *Am. Chem. Soc. Symp. Ser.*, 1985, **288**, 280.
3 M. G. Samant and M. Boudart, *J. Phys. Chem.*, 1991, **95**, 4070.
4 M. Vaarkamp, J. T. Miller, F. S. Modica and D. C. Koningsberger, *J. Catal.*, 1996, 163, 294.

5 M. Vaarkamp, PhD Thesis, Eindhoven University of Technology, Eindhoven, l996.
6 A. V. Soldatov, S. Della Longa and A. Bianconi, *Solid State Commun.*, 1993, **85**, 863.
7 K. Asakura, T. Kubota, N. Ichikuni and Y. Iwasawa, *Stud. Surf. Sci. Catal.*, 1996, **101**, 911.
8 S. N. Reifsnyder, M. M. Otten, D. E. Sayers and H. H. Lamb, *J. Phys. Chem. B*, 1997, **101**, 4972.
9 B. I. Boyanov and T. I. Morrison, *J. Phys. Chem.*, 1996, **100**, 16318.
10 B. Hammer and J. K. Nørskov, *Nature*, 1995, **376**, 238.
11 H. Yoshitake and Y. Iwasawa, *J. Phys. Chem.*, 1991, **95**, 7368; *J. Phys. Chem.*, 1992, **96**, 1329.
12 D. C. Koningsberger, F. B. M. van Zon, M. Vaarkamp and A. Muñoz-Paez, in *X-ray Absorption Fine Structure for Catalysts and Surfaces*, ed. Y. Iwasawa, Series on *Synchrotron Radiation Techniques and Applications*, World Scientific Singapore, 1996, vol. 2, p. 257.
13 N. Ichikuni and Y. Iwasawa, *Catal. Lett.*, 1993, **20**, 87.
14 B. L. Mojet, PhD Thesis, Utrecht University, Utrecht, 1997.
15 B. L. Mojet, M. J. Kappers, J. C. Muijsers, J. W. Niemantsverdriet, J. T. Miller, F. S. Modica and D. C. Koningsberger, *Stud. Surf. Sci. Catal.*, 1994, **84**, 909.
16 B. L. Mojet, M. J. Kappers, J. T. Miller and D. C. Koningsberger, *Stud. Surf. Sci. Catal.*, 1996, **101**, 1165.
17 R. J. M. J. Vogels, M. J. H. V. Kerkhoffs and J. W. Geus, *Stud. Surf. Sci. Catal.*, 1995, **91**, 1153.
18 F. W. H. Kampers, T. M. J. Maas, J. van Grondelle, P. Brinkgreve and D. C. Koningsberger, *Rev. Sci. Instr.*, 1989, **60**, 2645.
19 *X-ray Absorption*, ed. D. C. Koningsberger and R. Prins, John Wiley & Sons, New York, 1988.
20 J. W. Cook and D. E. Sayers, *J. Appl. Phys.*, 1991, **52**, 5024.
21 M. Vaarkamp, J. C. Linders and D. C. Koningsberger, *Physica B*, 1995, **208 & 209**, 159.
22 F. W. H. Kampers, PhD Thesis, Technische Universiteit Eindhoven, Eindhoven, 1988.
23 D. C. Koningsberger, in *Neutron and Synchrotron Radiation for Condensed Matter Studies*, ed. J. Baruchel, J. L. Hodeau, M. S. Lehmann, J. R. Regnard and C. Schlenker, *Applications to Solid State Physics and Chemistry*, Springer Verlag, 1994, vol. II. pp. 213–14.
24 L. F. Mattheiss and R. E. Dietz, *Phys. Rev. B*, 1980, **22**(4), 1663.
25 J. R. Taylor, *Scattering Theory: The quantum theory nonrelativistic collisions*, E. Krieger Publ. Comp., Florida, 1983, p. 243.
26 M. Vaarkamp, F. S. Modica, J. T. Miller and D. C. Koningsberger, *J. Catal.*, 1993, **114**, 611.
27 S. I. Zabinsky, J. J. Rehr, A. Ankudinov, R. C. Albers and M. J. Eller, *Phys. Rev. B*, 1995, **52**, 2995.
28 U. van Barth and G. Grossman, *Solid State Commun.*, 1979, **32**, 645.
29 J. Stohr, *NEXAFS Spectroscopy*, Springer-Verlag, Heidelberg, 1992.
30 J. P. Long, V. M. Bermudez and D. E. Ramaker, *Phys. Rev. Lett.*, 1996, **76**, 991.
31 R. A. van Santen, *J. Chem. Soc., Faraday Trans. 1*, 1987, **83**, 1915.

Paper 9/00716D